J Low Temp Phys (2014) 176:749–754
DOI 10.1007/s10909-013-1066-4

Optical Efficiency and R(T,I) Measurements of ACTPol TESes Using Time Domain Multiplexing Electronics

C. G. Pappas · J. Beall · J. Brevick · H. M. Cho · M. J. Devlin · A. Fox · E. A. Grace · G. C. Hilton · J. Hubmayr · K. D. Irwin · J. Klein · D. Li · M. Lungu · L. B. Newburgh · J. P. Nibarger · M. D. Niemack · J. J. McMahon · L. A. Page · B. L. Schmitt · S. T. Staggs · J. Van Lanen · E. J. Wollack

Received: 31 July 2013 / Accepted: 23 December 2013 / Published online: 15 January 2014

Abstract We present new data on feedhorn-coupled transition-edge sensor devices fabricated for the second-generation receiver (ACTPol) for the Atacama cosmology telescope (ACT). First, we describe optical efficiency measurements of the latest ACTPol detector wafer, which has a 86 ± 15 % average optical efficiency. Next, we discuss measurements of the TES resistance as a function of temperature and bias current ($R(T, I)$) using the ACTPol time-domain multiplexing electronics. Qualitative agreement between $R(T, I)$ data at low bias current and the two-fluid model prediction is

C. G. Pappas (✉) · E. A. Grace · L. A. Page · S. T. Staggs
Department of Physics, Princeton University, Jadwin Hall, Princeton, NJ 08544, USA
e-mail: cpappas@princeton.edu

M. D. Niemack
Department of Physics, Cornell University, Ithaca, NY 14853, USA

E. J. Wollack
Goddard Space Flight Center, 8800 Greenbelt Rd, Greenbelt, MD 20771, USA

J. J. McMahon
Department of Physics, University of Michigan, 1440 Randall Lab, 450 Church Street, Ann Arbor, MI 48109-1040, USA

J. Beall · J. Brevick · H. M. Cho · A. Fox · G. C. Hilton · J. Hubmayr · K. D. Irwin · D. Li · J. P. Nibarger · J. Van Lanen
Quantum Electronics and Photonics Division, National Institute of Standards and Technology, Boulder, CO 80305, USA

M. J. Devlin · J. Klein · M. Lungu · B. L. Schmitt
Department of Physics and Astronomy, University of Pennsylvania, 209 South 33rd Street, Philadelphia, PA 19104-6396, USA

L. B. Newburgh
Department of Astronomy and Astrophysics, University of Toronto, 50 St. George St, Toronto, ON M5S 3H4, Canada

shown. Using the two-fluid model and low bias current $R(T, I)$ data, α and β at our operating bias current are calculated.

Keywords Transition edge sensor (TES) · Cosmic microwave background (CMB) · Polarization · Atacama cosmology telescope · ACTPol

1 Introduction

ACTPol is the polarization-sensitive, second-generation receiver for the Atacama Cosmology Telescope (ACT) located in the Atacama Desert, Chile [1,2]. It will have three 1000 TES detector arrays: two with 150 GHz detectors, and one with multichroic 90/150 GHz detectors [3]. Observations have recently begun with the first 150 GHz array [4]. In this paper, we present optical efficiency and $R(T, I)$ data from the testing and characterization of detectors for the second 150 GHz array.

2 Optical Efficiency Measurements

ACTPol pixels, fabricated at NIST, are designed to minimize signal loss. Compared to the previous NIST pixel design, improvements have been made by shortening the microstrip lines and removing on-chip filters [5]. Sources of signal loss in ACTPol type detectors include impedance mismatches in transmission lines and absorption of the signal by silicon oxide (SiOx) dielectric. The detectors discussed in this paper have a 0.0026 SiOx loss tangent at 6–9 GHz according to resonator measurements. From simulations, we expect ACTPol detectors with this loss tangent at frequencies in our 150 GHz band to have optical efficiencies of 85 %.

The optical efficiencies of detector wafers under consideration for use in ACTPol are tested with a heated blackbody cold load radiation source. The radiation passes through a bandpass filter centered at 150 GHz before reaching the detectors. The optical efficiency is measured by taking current vs. voltage (IV) curves at various cold load temperatures and calculating P_{el}, the amount of electrical power needed to bias the TES to 90 % of the normal resistance, as a function of photon power incident on the detector. The total power flowing to the bath, P_{sat}, is taken to be a constant. As the amount of radiation absorbed by the detectors increases, P_{el} decreases:

$$P_{el} = P_{sat} - \eta P_{\gamma}, \tag{1}$$

where P_{γ} is the amount of radiation incident on the detectors, and η is the optical efficiency, or the fraction of incident radiation detected. Because the ACTPol feedhorns are monolithically fabricated from array-size silicon wafers, they cannot be used for optical efficiency testing of individual wafers. Instead, we test with individually machined aluminum corrugated feedhorns [6]. The coupling of radiation through the feedhorns to the OMTs is known from simulations and included in the calculation of P_{γ}, such that η is the optical efficiency of the detectors only.

In Fig. 1, P_{el} vs. P_{γ} is plotted for 12 detectors on the latest ACTPol detector wafer at cold load temperatures of ∼4, ∼8, ∼12, and ∼16 K. The slopes of linear fits to

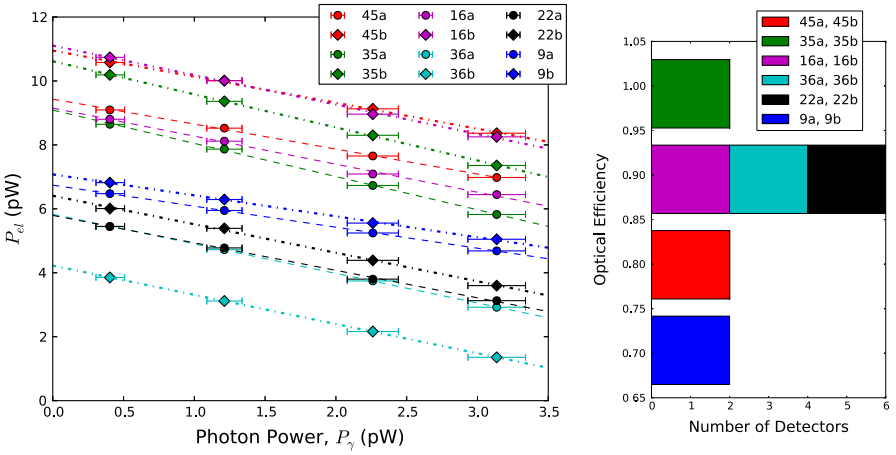

Fig. 1 *Left* P_{el} is plotted vs. P_γ for 12 detectors. The slope of the line fitted to the data is $-\eta$ (Eq. 1). *Numbers* in the legend refer to the pixel number. There are two detectors, a and b, on each pixel, one for each polarization. *Right* Optical efficiency results from data on *left*. Detectors on the same pixel differ by at most 4 % in optical efficiency (Color figure online)

the data give the detectors' optical efficiencies (Eq. 1). The systematic error on the optical efficiency measurement is ±15 %, and is mainly due to uncertainty in the cold load temperature. The average of the detectors' optical efficiencies, 86 %, matches the simulated optical efficiency, 85 %, within the error bounds.

3 $R(T, I)$ Measurements

The TES can be used as a very sensitive resistive thermometer due to its sharp temperature-driven resistive transition between the normal and superconducting states. By measuring $R(T, I)$ of TESes under consideration for use in ACTPol, we can see how the $R(T)$ curve evolves with changing bias current and look for non-linearities in the transition. For good performance, the logarithmic derivative of resistance with respect to current (β) will be small compared to its logarithmic derivitive with respect to temperature (α). Linearity of the R(T) function near the bias point is necessary for accurate TES calibration.

To date, the transition shapes of TESes have been described by the two-fluid model [8,9] and the resistively shunted junction (RSJ) model, wherein high T_c electrodes proximitize the lower T_c TES [10,11]. The ACTPol TESes are 54.0 μm wide × 76.5 μm long molybdenum-copper bilayer films with copper bars on the sides of the film. Due to the small size of the ACTPol TESes and the fact that we use high T_c niobium electrodes, it is possible that they may exhibit some weak link behavior described by the RSJ model [10–12]. In this paper, we explore how well the $R(T, I)$ behavior can be understood in terms of the two-fluid model.

The two-fluid model is based on the Skocpol–Beasley–Tinkham (SBT) model [13], which accurately describes the transition of type I superconducting films. In the

two-fluid model description of the TES transition, the TES current, I_{TES}, is carried partially by normal electrons and partially by superconducting electrons:

$$I_{TES} = I_n + I_{sc} = I_n + c_I(T, I)I_c(T) = I_n + c_I(T, I)I_{co}(1 - T/T_c)^{3/2}, \quad (2)$$

where the superconducting current is some fraction, c_I, of the Ginzburg–Landau (GL) critical current, $I_c(T)$. Because the superconducting current is dissipationless, the voltage measured in the transition region is due only to the normal current. The resistance on the normal electrons is some fraction, c_R, of R_n, giving:

$$R_{TES}(T, I_{TES}) = \frac{c_R R_n I_n}{I_{TES}} = c_R(T, I_{TES})R_n\left(1 - c_I(T, I_{TES})I_{co}\frac{(1 - T/T_c)^{3/2}}{I_{TES}}\right). \quad (3)$$

In the most general treatment of the two-fluid model, $c_I(T, I)$ and $c_R(T, I)$ are functions that may depend weakly on temperature and current. Here, we will follow Irwin et al [8] and, in a slight simplication to the SBT model, take c_R and c_I to be constants: $c_R = 1$ and $c_I = 1/2$. In this case, the $R(T)$ transition at constant I_{TES} is driven only by the critical current's temperature dependence, with the shape of the $R(T)$ curve depending on the magnitude of I_{TES}.

In the ACTPol bias configuration, the TESes are effectively voltage biased to provide negative electrothermal feedback, keeping the TES in its transition region as the CMB signal fluctuates. This is achieved by current biasing the TES in parallel with a shunt resistor of 0.18 mΩ, about 28 times smaller than the normal resistance of the TES. By measuring I_{TES}, at a given total bias current, I_{bias}, we measure the resistance of the TES, R_{TES}: $R_{TES} = R_{sh}\left(\frac{I_{bias}}{I_{TES}} - 1\right)$. The readout and amplification of the TES current is provided by a three-tiered time domain SQUID multiplexing system, coupled to an inductor in series with the TES. [15]

For three TESes, TES A, TES B, and TES C, $R_{TES}(T)$ was measured as a function of increasing and decreasing temperature sweeps of 0.04 mK/min at constant DC I_{bias} values of 2.8, 5.3, 9.1, 15.4, and 21.7 μA. As shown for TES A in Fig. 2, no hysteresis was observed in the TESes measured; $R(T)$ curves from increasing and decreasing temperature sweeps match within the measurement error. In terms of I_{bias} and temperature, R_{TES} predicted by the two-fluid model can be written as:

$$R_{TES}(T, I_{bias}) = \left(\frac{I_{bias} - c_I I_c(T)}{I_{bias}/(c_R R_n) + c_I I_c(T)/R_{sh}}\right). \quad (4)$$

By measuring the function $c_I * I_c(T)$, we can calculate $R(T, I)$ predicted by the two-fluid model and compare to the data. When R_{TES} first becomes non-zero with increasing temperature or first becomes zero with decreasing temperature, we define I_{bias} as $c_I * I_c(T)$ at that temperature. As shown in Fig. 3, if we assume c_I is constant over the current and temperature range of the data, the critical current data follow the GL theoretical expression for $I_c(T)$ (Eq. 2). Although we do not see evidence in these data for deviations from GL theory due to weak-link effects, as observed by Sadleir et al. [10], future measurements of $I_c(T)$ over a broader temperature range are needed to rule out this possibility.

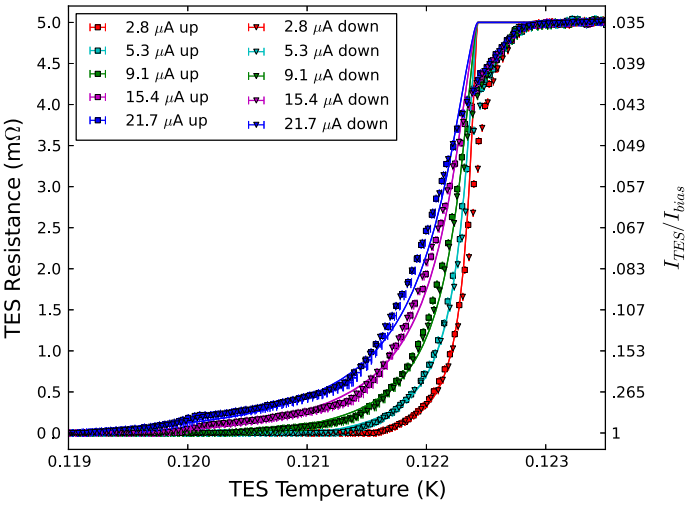

Fig. 2 For TES A, R_{TES} vs. Temperature at constant I_{bias}. For each I_{bias} value, $R(T)$ data for an increasing (*up*) and decreasing (*down*) temperature sweep are shown. On the second y-axis, I_{TES}/I_{bias} is shown. Positive *error bars* on T_{TES} are calculated from P_h and a lower bound estimate on the thermal conductivity between the TES island and the bath. Solid lines are two-fluid model $R_{TES}(T, I_{bias})$ (Eq. 4) predictions using $c_I = 1/2$, $c_R = 1$, and $I_c(T)$ data (Color figure online)

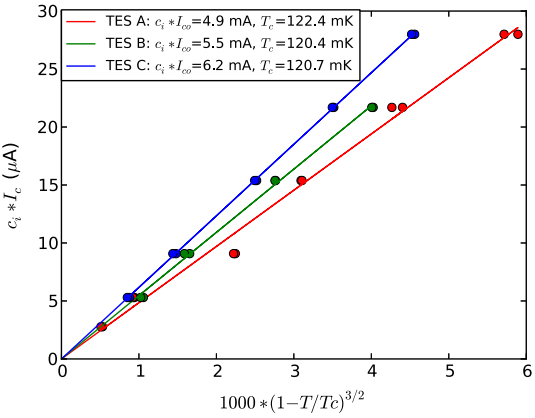

Fig. 3 $c_I\, I_c(T)$ is plotted vs. $1000 * (1 - T/T_c)^{3/2}$ for TESes A, B, and C. Assuming c_I is constant over this range, the $I_c(T)$ data follows the GL theoretical $I_c(T)$ function, as shown by the linear fits to the data. In the legend, T_c and $c_I * I_{co}$, found from the linear fits, are shown for each detector (Color figure online)

From $c_I * I_c(T)$, theoretical $R(T)$ curves from the two-fluid model (Eq. 4) with $c_R = 1$ are calculated for TES A and plotted over the data in Fig. 2. There is qualitative agreement between the data and the curves from the two-fluid model up to about 80 % R_n. The agreement is especially good for the curves at the lowest I_{bias} values, and starts to deviate at higher I_{bias} as the transition widens and slight anomolies in the R(T) curve emerge.

The $R(T)$ curves shown in Fig. 2 were taken at low I_{bias} such that electrical power on the TES, P_h, was minimal ($P_h < 0.02$ pW) and $T_{TES} = T_{bath}$. As I_{bias} is increased, the temperature at which a given resistance occurs shifts to lower temperatures, as predicted by the two-fluid model. It is evident from this trend that the resistance

values at typical operating I_{bias} of ∼1 mA, where P_h ∼10 pW and a direct $R(T)$ measurement is not possible, would be shifted to even lower temperatures than those measured at low I_{bias} shown here.

Although a direct measurement of $R(T)$ is not possible at typical operating I_{bias} values due to heating effects, we can predict $R(T)$ curves and TES parameters at these higher I_{bias} values with the two-fluid model. For an I_{bias} of 1 mA, using the two-fluid model with $c_R = 1$ and our $c_I * I_c(T)$ data, we calculate α at $R_n/2$ and $T(R_n/2)$, the temperature at which $R_{TES} = R_n/2$. For TESes A, B, and C, respectively, $\alpha = 40$, 43, and 47, and $T(R_n/2)/T_c = 96$, 96, and 97 %. Regardless of bias current, the two-fluid model with $c_R = 1$ predicts $\beta = 1$ at $R_n/2$. Future work will include complex impedance measurements of α and β at higher I_{bias} to compare to the two-fluid model predictions here (see, e.g., Zhao [16]).

4 Conclusions

We find an average optical efficiency of 86 ± 15 % for the latest fabricated detector wafer under consideration for the ACTPol second 150 GHz array. The $I_c(T)$ data of three TESes with smooth $R(T)$ transitions show a temperature dependence predicted by the GL theory, in agreement with the two-fluid model. Using the measured $c_I * I_c(T)$ data and c_R=1, the two-fluid model gives $R(T, I)$ predictions that qualitatively match the data and α's of 40, 43, and 47 at $R_{TES} = R_n/2$ and I_{bias} = 1 mA .

References

1. M.D. Niemack et al., in *Proceedings of the SPIE 77411S*, p. 21, 2010
2. K.M. Smith et al., arXiv:0811.3916 (2008)
3. R. Dattar et al., this special issue LTD15 in J. Low Temp. Phys.
4. E. Grace et al., this special issue LTD15 in J. Low Temp. Phys.
5. D. Li et al., IEEE Trans. Appl. Supercond. **23**, 1501204 (2013)
6. K. Visnjic, Princeton University, PhD Thesis, 2013
7. K. Irwin, G. Hilton, Transition-edge sensors, *Cryogenic Particle Detection* (Springer-Verlag, Berlin, 2005)
8. K.D. Irwin, G.C. Hilton, D.A. Wollman, J.M. Martinis, J. Appl. Phys. **83**, 3978 (1998)
9. D.A. Bennett, D.S. Swetz, R.D. Horansky, D.R. Schmidt, J.N. Ullom, J. Low Temp. Phys. **167**, 102 (2012)
10. J.E. Sadleir, S.J. Smith, S.R. Bandler, J.A. Chervenak, J.R. Clem, Phys. Rev. Lett. **104**, 047003 (2010)
11. A. Kozorezov et al., Appl. Phys. Lett. **99**, 063503 (2011)
12. D.A. Bennett, D.S. Swetz, D.R. Schmidt, J.N. Ullom, Phys. Rev. B **87**, R020508 (2013)
13. W.J. Skocpol, M.R. Beasley, M. Tinkham, J. Low Temp. Phys. **16**, 145 (1974)
14. M. Tinkham, *Introduction to Superconductivity* (Dover Publications, Mineola, 1996)
15. J.A. Chervenak, K.D. Irwin, E.N. Grossman, J.M. Martinis, C.D. Reintsema, M.E. Huber, Appl. Phys. Lett. **74**, 4043 (1999)
16. Y. Zhao, Princeton University, PhD Thesis, 2010